ELSEVIER

Contents lists available at ScienceDirect

Earth and Planetary Science Letters

www.elsevier.com/locate/epsl



Fracturing and pore-fluid distribution in the Marlborough region, New Zealand from body-wave tomography: Implications for regional understanding of the Kaikōura area



Benjamin A. Heath ^{a,b,*}, Donna Eberhart-Phillips ^{c,d}, Federica Lanza ^e, Clifford Thurber ^a, Martha K. Savage ^f, Tomomi Okada ^g, Satoshi Matsumoto ^h, Yoshihisa Iio ⁱ, Stephen Bannister ^d

- ^a University of Wisconsin-Madison, Madison, WI, USA
- ^b National Tsunami Warning Center, Palmer, AK, USA
- ^c University of California-Davis, Davis, CA, USA
- ^d GNS Science, Lower Hutt, New Zealand
- ^e Swiss Seismological Service, ETH-Zürich, Zürich, Switzerland
- ^f Victoria University of Wellington, Wellington, New Zealand
- g Tohoku University, Sendai, Japan
- h Kyushu University, Fukuoka, Japan
- ⁱ Kyoto University, Uji, Japan

ARTICLE INFO

Article history:
Received 25 December 2021
Received in revised form 3 June 2022
Accepted 6 June 2022
Available online 27 June 2022
Editor: R. Bendick

Keywords: tomography fracturing tectonics fault maturation pore-fluid New Zealand

ABSTRACT

Relative to more mature fault zones, immature fault zones that have accumulated smaller total displacement are characterized by less efficient strain localization and more complicated earthquake ruptures. How differences in maturation are reflected in regional-scale upper-crustal fracturing is not well known. Recently, complicated earthquake ruptures associated with immature fault zones, such as the 2016 Kaikōura earthquake in New Zealand, have occurred in areas that are in regional proximity (<100 km away) to more mature faults. Here we examine whether inefficient strain localization in less mature fault zones is associated with a broader distribution and anomalously elevated concentration of fractures over distances of tens of kilometers. We use regional seismic arrival-time tomography in a broad area around the Kaikōura earthquake to investigate lateral variations in Vp and Vp/Vs. Focusing on the extensively faulted but compositionally uniform Torlesse-Pahau terrane in the Marlborough region where the earthquake occurred, we attribute lateral variations in Vp and Vp/Vs to differences in concentration of fluid-filled fractures. Using numerical models relating seismic velocities and fracturing, we solve for the lateral variation in concentration of \sim 0.01 aspect ratio fluid-filled fractures. We find that areas near the Kaikōura rupture have >3% elevated fracture porosity compared to the adjacent area to the north. The elevated regional fracturing in the Kaikoura area is interpreted to result from more distributed deformation, and broader distribution of earthquakes, due to inefficient localization of strain from a regionally uniform strain rate field, highlighting the relationship between relative maturity of uppercrustal fault zones and lateral variability of regional upper-crustal properties.

Plain language summary:

When earthquakes occur in immature fault zones (areas that have accumulated small total displacement), they tend to rupture multiple poorly developed faults of diverse orientations. In contrast, more mature fault zones are associated with more developed, smoother faults and more localized earthquake activity. How these differences in maturation are reflected in the regional distribution of fractures is not well known. Here we use the arrival times of P and S waves from earthquakes to constrain seismic velocities (Vp and Vp/Vs) and use numerical models to relate seismic velocities to fracture concentration. We focus on the Marlborough region of the South Island, New Zealand, where immature fault zones recently ruptured during the 2016 Kaikōura earthquake but which also has more mature fault zones <100 km away. We find elevated fracture concentrations (3% higher fracture porosity), indicative of more distributed deformation along immature fault zones relative to more mature fault zones. In immature

^{*} Corresponding author at: National Tsunami Warning Center, Palmer, AK, USA. E-mail address: benjamin.heath@noaa.gov (B.A. Heath).

settings, fracturing is not as effectively localized along individual fault traces, leading to a broadly distributed fracture network.

Published by Elsevier B.V.

1. Introduction

The growth of major faults that span 100s of km is thought to start from the interaction and coalescence of microfractures, where initially broadly distributed microfractures localize into faults, which then subsequently coalesce to form through-going fault zones and regional fault systems (Reches and Lockner, 1994; Cowie et al., 1995). The impact of maturation of individual major faults on crustal structure for distances less than one hundred meters from the fault is reasonably well understood: increased offset leads to smoothing of fault traces, decreased off-fault deformation, and a more localized geometry of strain accommodation along the main fault (Kim et al., 2004; Faulkner et al., 2010; Dolan and Haravitch, 2014). However, how this maturation process is manifested in the regional upper crustal structure further from the fault, for example the distribution of fractures over distances of tens of kilometers from faults, is not well known.

The maturation of major faults is typified in the Marlborough region of New Zealand, where older faults have accumulated larger displacements (e.g. Little and Jones, 1998) and subsequently tend to have simpler geometries (e.g. Rattenbury et al., 2006) and less off-fault deformation (e.g. Zinke et al., 2015) than their less mature counterparts. The more mature faults tend to be located in the northern portion of the Marlborough region (Little and Jones, 1998). In contrast, the southern portion of the Marlborough region is characterized by less mature faults, such as the faults that ruptured during the 2016 Kaikōura earthquake. These faults have diverse orientations, complicated fault traces, and are hypothesized to be associated with elevated concentrations of over-pressured pore fluids (Hamling et al., 2017; Litchfield et al., 2018; Ulrich et al., 2019; Sibson, 2020). The lateral variation in fault zone maturity within the broad Marlborough region makes it an ideal setting for investigating the effect of maturation on regional crustal structure.

A common way of understanding the differences in regional structure over tens of km is through interpretation of variations in seismic velocities, specifically Vp and Vp/Vs. However, interpretations based on Vp and Vp/Vs are complicated by non-uniqueness. Variations can be due to differences in lithology/composition (Zandt and Ammon, 1995; Christensen, 1996; Shillington et al., 2013), fracturing (Takei, 2002; Kim et al., 2019b), fluid pressure (Eberhart-Phillips and Reyners, 1997; Hudson, 2000), or a combination of the above (Thurber et al., 1997; Zhang et al., 2009). Moreover, although these factors can vary independently, they also may be correlated. For example, the distribution of fault damage can be composition-dependent (e.g. Williams et al., 2016).

Here we use regional earthquake seismic tomography to constrain the regional Vp and Vp/Vs structure of the Marlborough region, leveraging the differences in accumulated fault offset of major faults to understand the associated impact of the process of maturation on regional crustal structure. In order to limit the role of composition as a source of velocity variation, we take advantage of the known basement structure to focus on only one broadly distributed lithology, the graywacke/metagraywacke of the Torlesse-Pahau terrane, limiting plausible interpretations of velocity variation. We map the regional variation of fracturing concentration via quantitative modeling of the effect of fluid-filled fractures on seismic velocity (Kim et al., 2019a), relating our interpretations of correlated Vp and Vp/Vs variations to the evolution of fracturing during the associated fault zone maturation process.

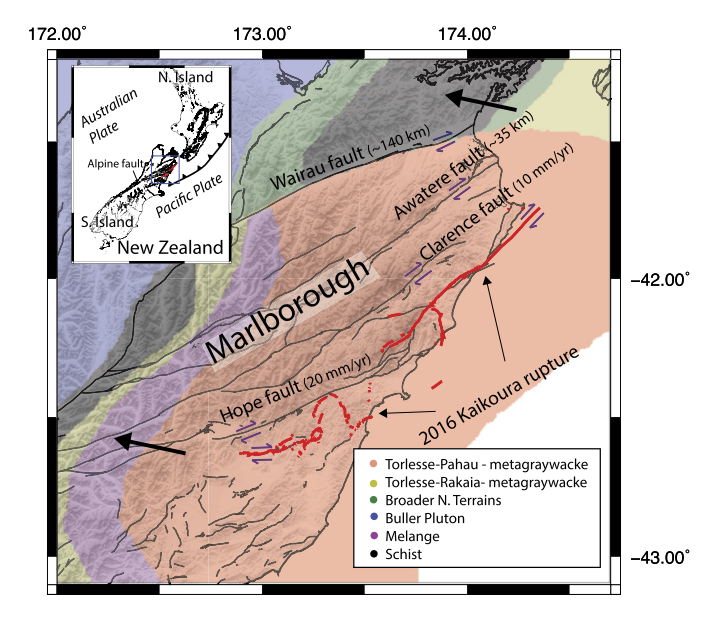


Fig. 1. Overview of the broader Marlborough region. Major faults (black lines) are labeled with slip rates (for the Hope and Clarence faults) and accumulated slip (for the Awatere and Wairau faults) (Knuepfer, 1992; Little and Jones, 1998). Red lines show the surface rupture of the 2016 Kaikōura earthquake (Litchfield et al., 2018). Regions are color-coded based on estimated basement lithology (Rattenbury et al., 2006). Orientation of maximum horizontal compression direction, from Haines and Wallace (2020), shown by bold black arrows. Inset shows regional setting in New Zealand.

2. Background

2.1. Regional setting

Here we highlight the regional basement structure in the northeastern portion of the South Island of New Zealand, Although the basement composition does, in general, vary laterally across the South Island, the composition is largely uniform within the Marlborough region and is characterized by a graywacke/metagraywacke composition referred to as the Torlesse-Pahau formation (Fig. 1) (Rattenbury et al., 2006). Minor deviations in composition from the graywacke do exist, including transitions to basalts, mudstones, and conglomerates; however, the unit has no consistent younging direction and there is a near uniform metamorphic grade (Rattenbury et al., 2006). Therefore, we consider these variations in composition within the Torlesse-Pahau terrain to be negligible in the context of this study, in which interpretations are on the broad scale of tens of kilometers. We focus specifically on Vp and Vp/Vs variations within this unit, capitalizing on the relative uniformity of the unit to exclude compositional variability as the source of lateral variations in seismic velocity. A similar approach has been used in magnetotellurics studies to exclude composition as a main driver of lateral variability in resistivity in the Marlborough region (Wannamaker et al., 2009).

The broader Marlborough region is juxtaposed between subduction of the Pacific plate beneath the Australian plate to the northeast and transpression along the Alpine Fault to the southwest (Fig. 1) (Walcott, 1998). The evolving tectonic setting in Marlborough is reflected in overall right-lateral transpression extending across numerous, mainly NE-SW oriented faults. The region ex-

periences a near uniform shear strain rate, with broad shearing throughout Marlborough extending down to the Alpine fault to the southwest (Haines and Wallace, 2020). Within the Marlborough region, the direction of maximum contraction is oriented approximately WNW, oblique to the regional faults (Haines and Wallace, 2020). The bulk of the relative plate motion between the Pacific and Australian plates in this region is accommodated by transpression-induced strike-slip and thrust motion along the Marlborough faults, as opposed to along the underlying subduction interface (Bibby, 1981; Walcott, 1998; Bourne et al., 1998a).

Within the upper crust, the broader Marlborough region is characterized by several major NE-SW trending faults: from north to south, the Wairau, Awatere, Clarence, and Hope faults (Fig. 1). These sub-parallel faults represent varying degrees of maturity. Broadly, the region to the north is characterized by more mature, well-developed faulting, whereas the region to the south is characterized by less mature faulting. The farthest north and most mature Wairau fault has accommodated most of the relative motion transferred by the Alpine fault (Yeats and Berryman, 1987; Walcott, 1998; Little and Jones, 1998). The lateral variability in maturation has consequences for the state of the crust. For example, comparison of the Wairau and Awatere faults reveals that the more mature Wairau fault is associated with more localized slip and a narrower region of off-fault deformation on scales of hundreds of m (Zinke et al., 2015).

Recently, the 2016 Kaikōura earthquake occurred along less mature faults in the southern portion of the Marlborough region (Fig. 1). This earthquake represents one of the most complex earthquakes ever recorded, rupturing multiple faults (>20) across a relatively broad area, and apparently not rupturing the adjacent Hope fault (Hamling et al., 2017; Litchfield et al., 2018) (Fig. 1). The rupture occurred in a region characterized by high fluid concentrations as well as elevated fracture/fault density (Eberhart-Phillips and Bannister, 2010; Ulrich et al., 2019; Sibson, 2020; Eberhart-Phillips et al., 2021).

2.2. Crustal fluids in the Marlborough region

Fluids are thought to play a critical role in active tectonic systems, particularly in earthquake processes. Elevated pore-fluid pressures lower the effective normal stress, enabling earthquake rupture at lower differential stresses (Rice, 1992; Sibson, 2020). With lower differential stresses required for rupture, the likelihood increases that any individual, non-optimally oriented fault can rupture (Okada et al., 2019; Sibson, 2020). As a result, complicated rupture patterns with diverse, non-optimally oriented fault orientations, such as those observed at Kaikōura, are commonly associated with the presence of fluids (Sibson, 2020). Without these fluids, higher effective normal stresses would inhibit rupture of non-optimally oriented faults, leading to rupture of faults with a more optimal orientation.

Studies of fault zones routinely find evidence for fluids in both the brittle upper-crustal layer as well as in shear zones at depth (McCaig, 1988; Rice, 1992; Faulkner et al., 2010). Upper crustal fluids are distributed both within the fault core, along the high permeability broader damage zone (Faulkner et al., 2010), and within the lower permeability surrounding crust (Rice, 1992). These fluids are either (a) supplied from below through ductile shear zones, with sources ranging from metamorphic and magmatic reactions, sediment dewatering, or fluids rising from the mantle, or (b) supplied from above via meteoric water (Kerrich, 1986; McCaig, 1988; Rice, 1992). In the Marlborough region, near Kaikōura, fluids are thought to result from mechanical dewatering and breakdown of clay as well as slab dehydration (Eberhart-Phillips and Reyners, 1997; Eberhart-Phillips and Henderson, 2004; Wannamaker et al., 2009; Okada et al., 2019). The distribution of fluids within the

broader crust is, in general, controlled by a combination of locations of sources of fluids, crustal permeability, and proximity to faults (Rice, 1992).

The presence of fluids has been inferred around the Marlborough region from a number of different observations: (1) in the mid-to-lower crust, elevated Vp/Vs, lowered Vp, lowered Q, and elevated conductivity of weakened crust beneath major strike-slip faults indicates the presence of crustal fluids, likely from slab dehydration (Eberhart-Phillips and Reyners, 1997; Eberhart-Phillips and Henderson, 2004; Wannamaker et al., 2009; Okada et al., 2019; Eberhart-Phillips et al., 2021); (2) in the Kaikōura region at uppercrustal depths, elevated crustal conductivity suggests mechanical dewatering, breakdown of clays, and increased concentration of fractures (Wannamaker et al., 2009); (3) upper-crustal faults that ruptured during the Kaikōura earthquake are largely sub-optimally oriented to the regional stress field and are also associated with anomalously elevated Vp/Vs, both of which are thought to indicate the presence of fluids (Eberhart-Phillips and Bannister, 2010; Sibson, 2020); and (4) dynamic rupture simulations of the Kaikōura earthquake suggest the presence of overpressured fluids (Ulrich et al., 2019).

3. Methods and results

Our dataset includes >103,000 P arrivals and >33,000 S-P times (S arrival time - P arrival time for a given station/event pair). The dataset is based on the Henrys et al. (2020) earthquake and active source dataset, with the addition of arrival times from Kaikōura aftershocks (Lanza et al., 2019) and other regional earthquakes (Fig. 2). For the addition of Kaikōura aftershocks, we combined stations in the Kaikoura region from the Disaster Prevention Research Institute (DPRI) temporary network (Okada et al., 2019) with stations from the Lanza et al. (2019) dataset (Fig. 2). To determine arrival times and associated uncertainties for the merged Kaikōura aftershock dataset, we used REST, an iterative arrivaltime picking and event relocation algorithm, after the approach of Lanza et al. (2019). For the addition of regional earthquakes, we included events from the GEONET catalog that occurred in 2019-2020, a period when upgraded monitoring enabled better appraisal of earthquakes and their associated picks, leading to fewer mispicks and hence better locations. The improved quality of the 2019-2020 picks, relative to prior earthquakes, was confirmed by our quality control analysis described below.

To assess the suitability of these additional earthquakes for tomographic inversion, we plotted record sections of the data, with corresponding arrival times and synthetic picks (estimated arrival times based on an initial 3-D velocity model from Henrys et al. (2020) and initial event locations). We ranked each event based on the clarity of arrivals. Any event that was not temporally isolated (e.g., there were arrivals from 2 different local/regional events arriving within <20 s of each other) was discarded. Finally, we assessed whether the synthetics indicated that the event arrival times were correctly associated with the event. In particular, we only included events for which synthetic arrival times for the initial event hypocenters and initial velocity model were visually accurate on average to within a few seconds of the observed picks. This limits the inclusion of badly mis-picked and mis-associated data.

Arrival times were inverted using a modified version of simul2000 (Thurber and Eberhart-Phillips, 1999; Eberhart-Phillips and Reyners, 2012), solving for both Vp and Vp/Vs as well as earth-quake locations and origin times. We used a 3-D starting model based on the Henrys et al. (2020) final model but interpolated onto a finer grid in the region of Kaikōura aftershocks. The model had a minimum grid spacing of 5 km and 10 km in the X (NW-SE) and Y (NE-SW) directions, respectively, in the region surrounding

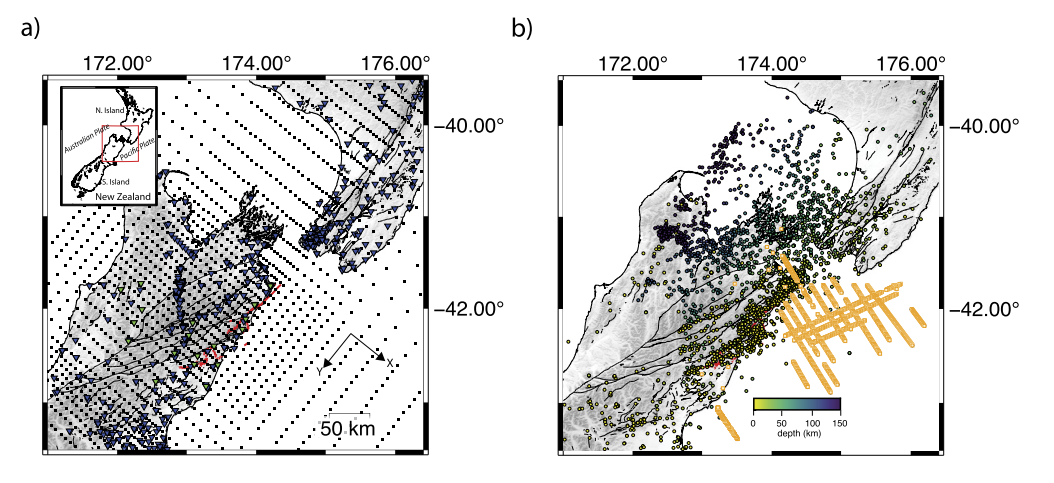


Fig. 2. a) Map of the study region, with regional faults shown as black lines and faults ruptured during the Kaikōura earthquake shown as red lines. Seismic stations included in the inversion are shown as blue and green triangles, with green triangles indicating DPRI seismic stations. Model nodes are shown as black dots. Inset shows New Zealand, with the red box outlining the map location. b) Plot of the distribution of earthquakes colored by depth (circles) as well as active sources (yellow squares). (For interpretation of the colors in the figure(s), the reader is referred to the web version of this article.)

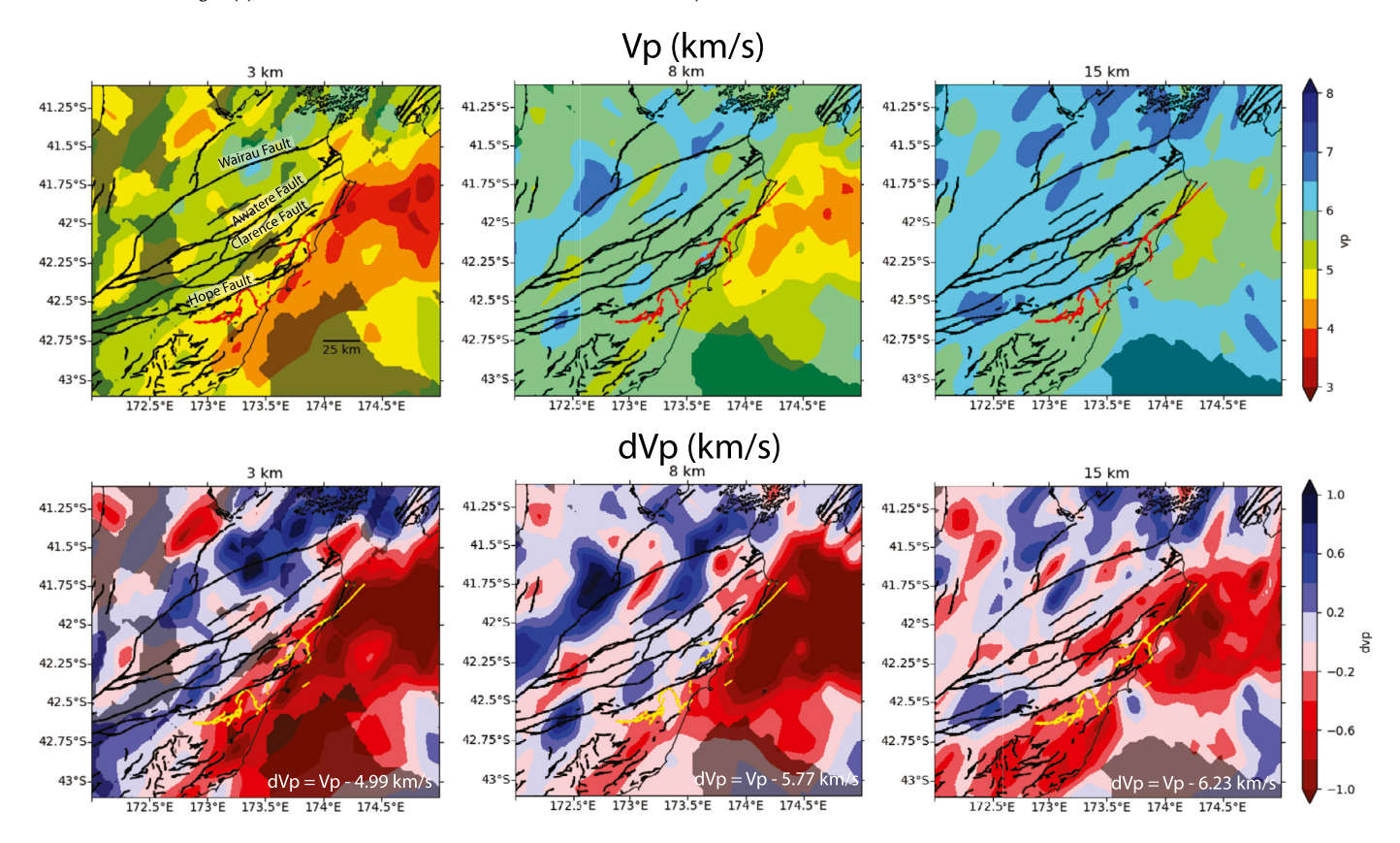


Fig. 3. Plots of Vp and dVp (Vp relative to a 1-D Vp regional average; see equation in lower right of dVp plots) at 3, 8, and 15 km depths, highlighting the Kaikōura region. Faults are as in Fig. 1. The Kaikōura region is characterized by, on average, anomalously low seismic velocities. The only area with lower seismic velocities is located offshore.

the Kaikōura aftershocks with spacing increasing away from the Kaikōura area (Fig. 2a). Using an L-curve, damping was selected to provide a substantial reduction in data misfit without excessive changes in velocity. To avoid overfitting the data, we performed only three iterations. Because our high-quality starting model already included substantial velocity heterogeneity required to fit the previous data set, the inversion yielded a 27% reduction in P data variance (final variance of 0.0342 s²) and 9% reduction in S-P data variance (final variance of 0.1583 s²) with respect to the 3-D starting model, resulting in a final weighted RMS residual of 0.219 s compared to a starting weighted RMS of 0.249 s in the 3-D starting model.

The final velocity models of Vp and Vp/Vs show several notable anomalies (Figs. 3 & 4). We present perturbations relative to a 1-D regional average, enabling easy visual comparison of relative velocity variations at different depths (3, 8, and 15 km below sea level), as well as absolute velocity, to enable correct physical interpretation. The region that ruptured during the Kaikōura earthquake is generally characterized by anomalously low Vp and elevated Vp/Vs, with approximately $-1~\rm km/s$ Vp and $+0.1~\rm Vp/Vs$ perturbations relative to the 1-D regional average (Figs. 3, 4, and S1). These perturbations transition towards $+1~\rm km/s$ Vp and $-0.08~\rm Vp/Vs$ over lateral distances of $\sim\!50~\rm km$ (Figs. 3, 4, 5, and S1). Although the amplitudes of perturbations at 3-15 km depth are relatively uni-

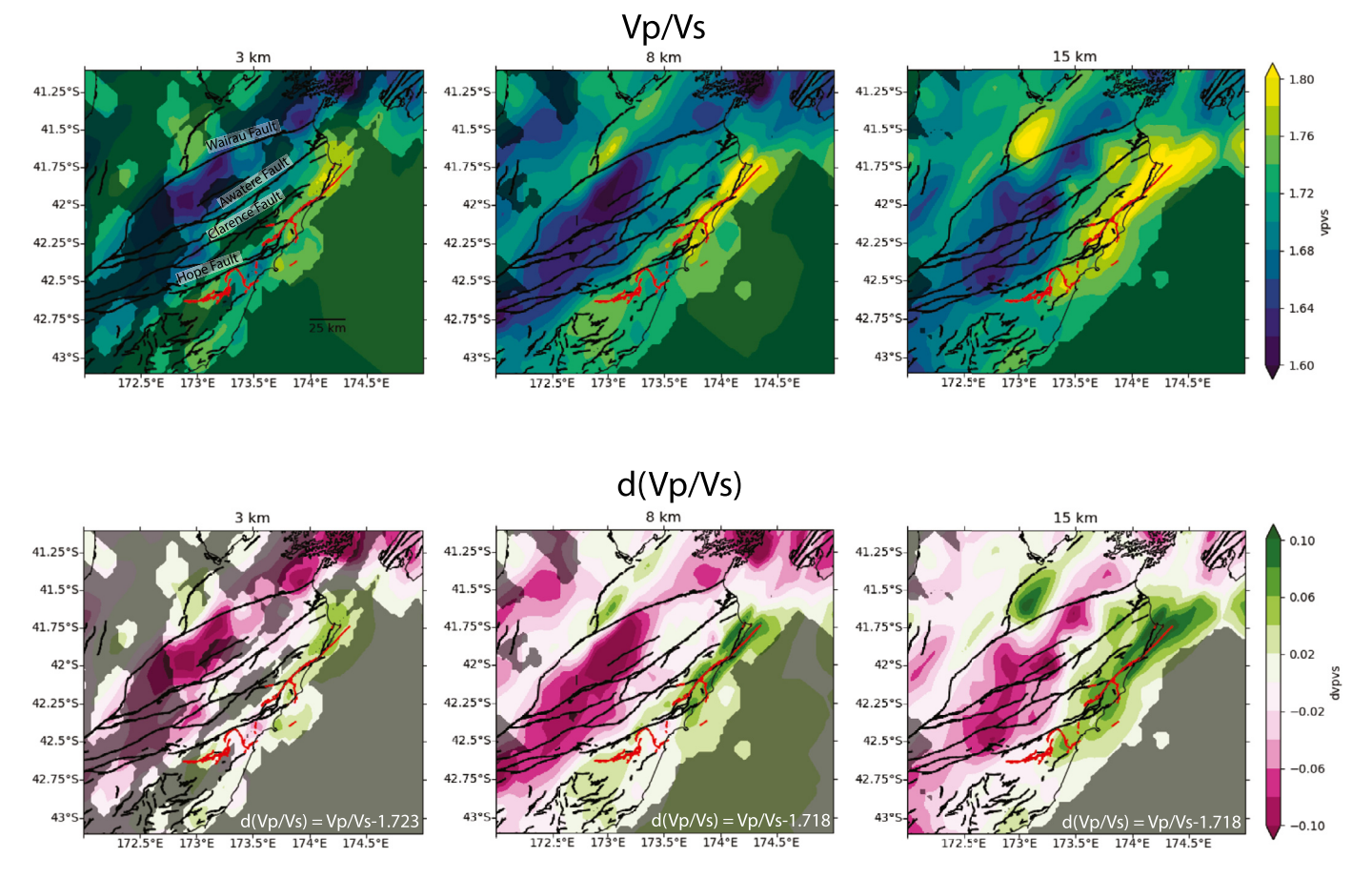


Fig. 4. Plots of Vp/Vs and d(Vp/Vs) (Vp/Vs relative to a 1-D Vp/Vs regional average; see equation in lower right of d(Vp/Vs) plots) at 3, 8, and 15 km. Faults are as in Fig. 1. We see anomalously elevated Vp/Vs values in the Kaikōura region.

form, the absolute velocities are not, due to the general increase in Vp with depth. For example, at 3 km depth, the Kaikōura region anomalies represent absolute values of \sim 4.5 km/s for Vp compared to values of \sim 5.5 km/s at 8 km depth.

Regional variations in velocity extending beyond Marlborough and the Torlesse-Pahau terrane compare well with regional changes in basement geology and crustal structure (Fig. 1, 3, and 4). Previous tomographic studies have shown that some of the New Zealand faults are associated with large differences in across-fault velocities, owing to a juxtaposition of rocks of differing lithology and hence different seismic velocities across the faults (Ellis et al., 2017). For example, the velocity difference in both Vp and Vp/Vs across parts of the Wairau fault at 8 km depth (Figs. 3 and 4) is attributed, in part, to changes in composition crossing from the graywacke/metagraywacke of the Torlesse-Pahau terrain to a high-grade schist (Fig. 1) (Eberhart-Phillips and Reyners, 1997). Similarly, variations in Vp and Vp/Vs in the southwestern portion of the study area correspond approximately with the transition from the Torlesse-Pahau terrain to compositionally different terrains (Figs. 1, 3, and 4). (Eberhart-Phillips and Reyners, 1997)

We focus on seismic velocity variations within the Torlesse-Pahau formation. There is substantial lateral variation in seismic velocity within this unit despite the relatively uniform composition, with lateral variations in Vp of >1.5 km/s and in Vp/Vs of >0.15. In Fig. 5, we plot average dVp and d(Vp/Vs) (perturbations with respect to the 1-D average seismic velocity model) relative to distance from faults ruptured during the Kaikōura earthquake, only including regions within the Torlesse-Pahau formation, finding an approximately linear increase in dVp and proportional decrease in d(Vp/Vs) over distances of 50 km. The ratio between the amplitude of the Vp and Vp/Vs perturbations is $\sim \! 10:1$, a result that synthetic

tests indicate is resolvable given the data coverage (Figs. S2 and S3).

We employ two techniques to understand sources of tomographically-resolved lateral variations in Vp and Vp/Vs in the Torlesse-Pahau formation: (a) we combine existing laboratory data on seismic velocities of different rock types (Okaya et al., 1995; Christensen, 1996) with known geologic structures (Rattenbury et al., 2006) to understand plausible variation in velocity from compositional differences due to both different lithologies and physical alteration of graywacke/metagraywacke, and (b) we use a numerical modeling technique to understand the impact of fluid-filled fractures on seismic velocity (Kim et al., 2019a). We elaborate on the numerical model below.

The numerical technique takes a starting medium and adds ellipsoidal fluid-filled inclusions of a given aspect ratio, yielding an effective medium that describes the seismic velocities as a function of fluid-filled inclusion volume fraction ($Vp(\phi)$, $\frac{Vp}{Vs}(\phi)$) for a given aspect ratio inclusion, where ϕ is fluid-filled inclusion volume fraction (Mainprice, 1997; Kim et al., 2019a). The results of the numerical forward model can be used to solve for the fracture concentration (fluid-filled inclusion volume) required to explain our recovered seismic velocities assuming all velocity variation results from fracturing. In the simplest form, at small volume fraction, $Vp(\phi)$ and $\frac{Vp}{Vs}(\phi)$ can be written as:

$$Vp(\phi) = Vp(\phi = 0) + \frac{\partial Vp}{\partial \phi}\Big|_{\phi=0} \phi$$
 (1)

$$\frac{Vp}{Vs}(\phi) = \frac{Vp}{Vs}(\phi = 0) + \frac{\partial \frac{Vp}{Vs}}{\partial \phi} \bigg|_{\phi = 0} \phi$$
 (2)

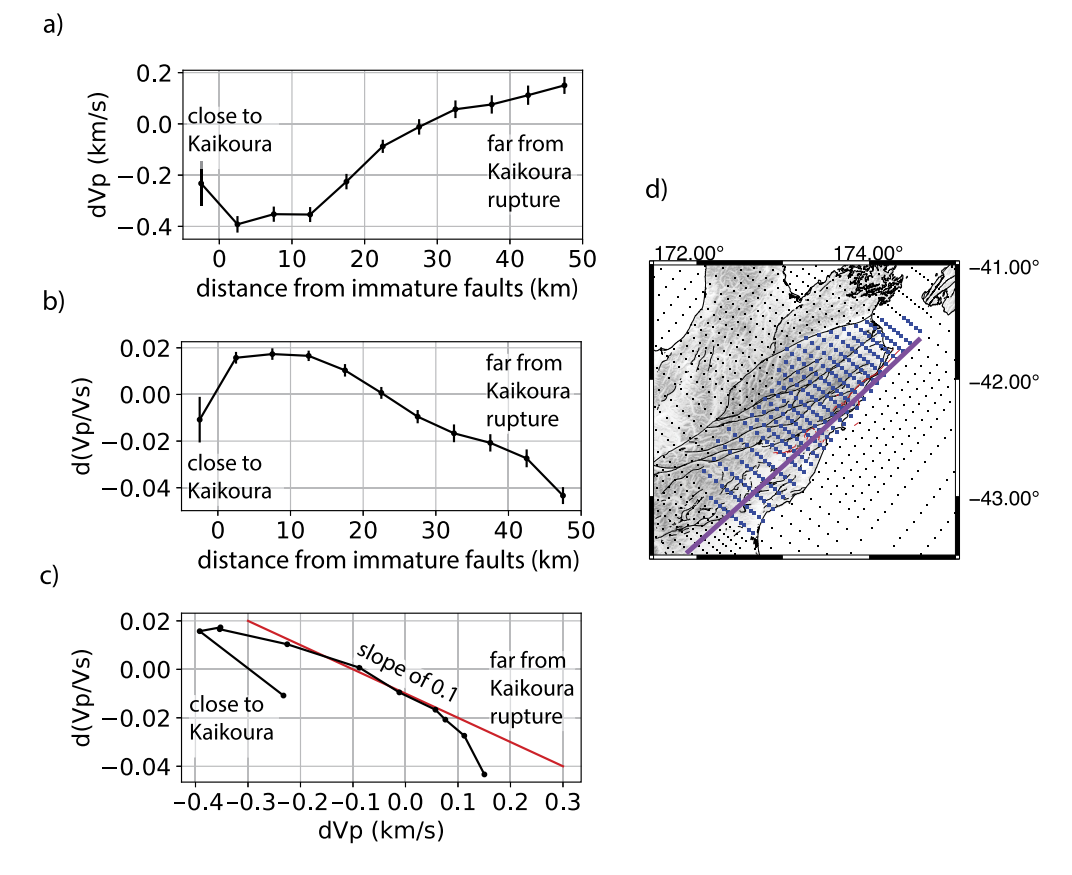


Fig. 5. Plot of a) dVp and b) d(Vp/Vs) (averaged over 0-15 km depths) as a function of the distance from area ruptured during the Kaikōura earthquake for well resolved regions within the Marlborough terrain (see (d) for location). c) Plot of dVp relative to d(Vp/Vs) from (a) and (b), with red line showing a slope of -0.1, indicating a 10 times larger variation in Vp compared to Vp/Vs. Areas near the active Kaikōura faults are characterized by lower Vp and higher d(Vp/Vs) in contrast to higher Vp and lower d(Vp/Vs) far from those faults. d) Inversion nodes (black), including well-resolved nodes within the Marlborough terrain used in (a), (b), and (c) (blue). Distance from immature faults (x axis in (a) and (b)) represents distance from the purple line in (d).

where $Vp\ (\phi=0)$ and $\frac{Vp}{Vs}\ (\phi=0)$ are the velocities of unfractured rock (assumed to be known), and the derivatives $(\frac{\partial Vp}{\partial \phi}|_{\phi=0})$ and $\frac{\partial \frac{Vp}{Vs}}{\partial \phi}|_{\phi=0}$ and obtained from the numerical modeling. Under the assumption that all the velocity variation results from fracturing, the tomographically recovered Vp at the ith velocity node is just $Vp_i = Vp\ (\phi=\phi_i)$ and $\frac{Vp}{Vs}$ at the ith node is just $\frac{Vp}{Vs} = \frac{Vp}{Vs}\ (\phi=\phi_i)$, where ϕ_i is the unknown fracture concentration in the vicinity of the ith node. Equations (1) and (2) therefore represent an overdetermined set of equations for fracture concentration at a given node (after assuming an aspect ratio), meaning we can use lateral variations in Vp and Vp/Vs to map the lateral variations in fracture concentration (see Text S1 for further information on the inversion procedure). Similar numerical models have been used to investigate fracturing at mid-ocean ridges as well as melt distribution at arc volcanoes (Kim et al., 2019b; Paulatto et al., 2019).

4. Discussion

4.1. Comparison to other geophysical studies

Several tomography studies have investigated the broader Marlborough region. The general tomographic findings presented here, of lowered Vp and elevated Vp/Vs in the Kaikōura area of the South Island, have been observed by a number of studies (Eberhart-Phillips and Reyners, 1997; Eberhart-Phillips and Bannister, 2010; Okada et al., 2019; Henrys et al., 2020), and were previously attributed to accumulated damage over multiple earthquake cycles and/or to increased pore-fluid pressures (Eberhart-Phillips and Reyners, 1997; Eberhart-Phillips and Bannister, 2015).

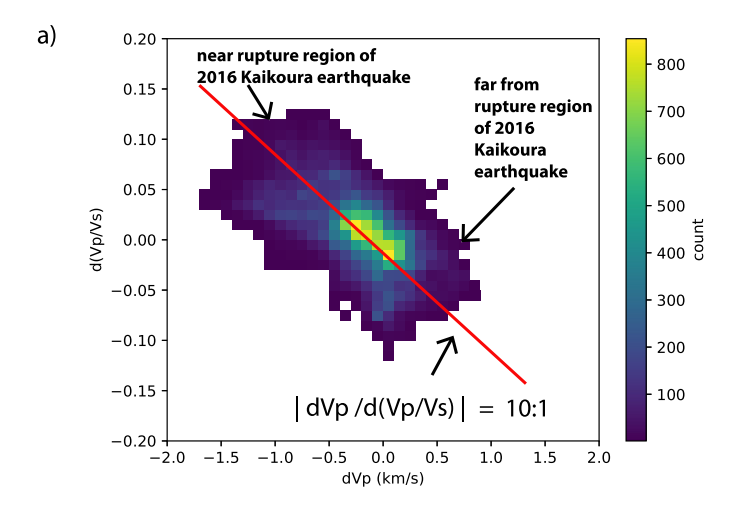
A 2-D magnetotellurics study, crossing from NW to SE within the Marlborough region, found upper crustal resistivities that are lower in the SE portion of Marlborough and higher in the NW (Wannamaker et al., 2009). This is consistent with our seismic velocities if lower Vp and elevated Vp/Vs are correlated with decreased resistivity, as predicted if both result from fractures filled with conductive fluids.

4.2. Sources of seismic velocity variability in the Marlborough region

We find a near-linear relationship between Vp and Vp/Vs anomalies within the Marlborough region, shown in a "heat-map" plot that represents the number of nodes in given ranges of dVp and d(Vp/Vs) values (Fig. 6). The amplitude of the respective low Vp, high Vp/Vs anomalies is found to be approximately proportional to the distance from the faults ruptured during the Kaikōura earthquake, with lowest dVp and highest d(Vp/Vs) in the Kaikōura area (Fig. 5). Below we discuss the role of composition and fracturing in explaining these observations.

The small role of composition on lateral variations in recovered Vp and Vp/Vs within the Torlesse-Pahau portion of the Marlborough region is confirmed by comparison to laboratory experiments for different lithologies and compositions. The highest velocities tomographically determined in the Marlborough region (high dVp/high Vp, low d(Vp/Vs)/low Vp/Vs) match the expected seismic velocities of graywacke/metagraywacke, the dominant rock type within the Torlesse-Pahau terrain for these depths (e.g., Eberhart-Phillips et al., 1989; Okaya et al., 1995; Christensen, 1996) (Fig. 6). For example, Christensen (1996) finds Vp of 5.83 km/s and Vp/Vs of 1.71 for pressures corresponding to depths of

Seismic Velocities of Part of the Torlesse -Pahau Formation



Compositional Variation - UNABLE to explain observed dVp and

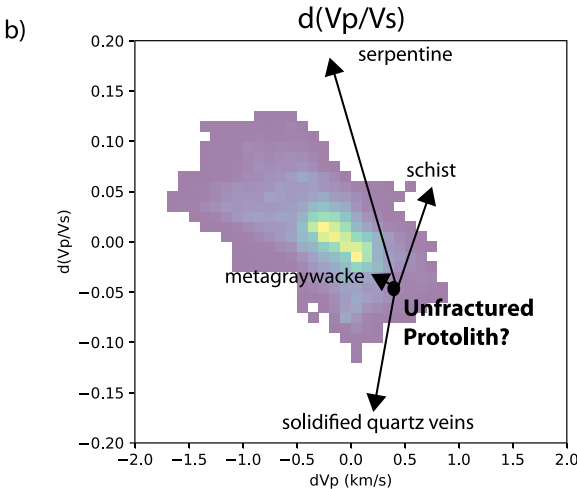


Fig. 6. a-b) Heat-map plots showing deviations in seismic velocity with respect to a 1-D regional average for depths from 0-15 km, focusing on the part of the Torlesse-Pahau formation near Kaikōura (Fig. 1). Similar to Fig. 5c, (a) shows that there is a linear relationship between dVp and d(Vp/Vs), with 10 times greater amplitude differences in dVp relative to d(Vp/Vs). Areas near the Kaikōura rupture have high d(Vp/Vs) and low dVp. b) The lowest d(Vp/Vs) and highest dVp values, here assumed to be an unfractured protolith, correspond approximately to the expected dVp and d(Vp/Vs) values for metagraywacke/graywacke (Okaya et al., 1995; Christensen, 1996), the lithology of the Torlesse-Pahau Formation. Compositional differences from this protolith are unable to explain the observations of high d(Vp/Vs) and lowered dVp elsewhere in the Torlesse-Pahau.

 \sim 8 km for metagraywacke, which equates to dVp of +0.06 km/s and d(Vp/Vs) of -0.01 (see Figs. 3 and 4). Okaya et al. (1995) find a slightly higher Vp of \sim 6.0 km/s for Torlesse graywacke at similar depths, yielding a dVp of \sim 0.23 km/s. While the highest velocities correlate well with graywacke/metagraywacke, the low dVp and high d(Vp/Vs) of the regions near Kaikōura are not easily explained by any individual composition, nor do these velocities match other lithologies present in the broader region (e.g. schist, Fig. 6). Compositional alteration, such as through serpentinization or quartz veins, also cannot explain our observations. Serpentinization, which can lower Vp and elevate Vp/Vs (Christensen, 1996), is not geologically plausible at upper crustal depths in the metagraywacke/graywacke terrain. Solidified quartz

veins, which could result from filled fractures, can lower Vp, but would also lower Vp/Vs (Mainprice, 1997) and therefore cannot explain the observation of elevated Vp/Vs. As no plausible lithology or compositional difference can easily explain the low Vp and high Vp/Vs near the Kaikōura rupture, the velocities likely result from physical alteration via fracturing of the high Vp, low Vp/Vs metagraywacke/graywacke.

Based on the evidence of regionally distributed fluids and their role in the Kaikōura rupture process (Eberhart-Phillips and Reyners, 1997; Ulrich et al., 2019; Sibson, 2020), we hypothesize that the inferred fractures suggested by lateral decreases in Vp and increases in Vp/Vs are fluid-filled. To constrain the distribution of fractures, we forward model the effect of different aspect ratio fractures with assumed ellipsoidal shape on the material stiffness tensor, which we then use to derive the associated seismic velocities of the medium (Kim et al., 2019a). In addition to varying the aspect ratio of inclusions, we also vary the concentration of inclusions, yielding seismic velocity as a function of fracture-induced porosity (ϕ) (Fig. 7). We find that the observed Vp and Vp/Vs variations can be jointly explained by variation in the concentration of fractures with 0.01 aspect ratio (Fig. 7). Such inferred fracture aspect ratios are consistent with aspect ratios determined in other studies (Crampin, 1986; Peacock and Hudson, 1990; Kim et al., 2019a). At a given depth in the Marlborough terrain, we infer that the areas of highest Vp and lowest Vp/Vs represent regions of metagraywacke/graywacke with the fewest fractures, whereas the regions of low Vp and high Vp/Vs represent areas of elevated fracture concentration.

For small fracture concentrations, numerical models show that the change in the volume of 0.01 aspect ratio fractures corresponds to linearly proportional changes in Vp and Vp/Vs with respect to unfractured rock (Kim et al., 2019a) (Fig. 7). We use the convention that dV is a perturbation with respect to a 1-D average and $\Delta V_{unfractured}$ is a perturbation with respect to the velocity of unfractured rock. By using inferred velocities for unfractured metagraywacke/graywacke and the observed dVp and d(Vp/Vs) values, we can solve equations (1) and (2) for approximate fracture concentration (see Kim et al. (2019a) and Text S1). We use the "heat maps" of dVp and d(Vp/Vs) to infer velocity anomalies for unfractured rock of dVp = 0.4 km/s and d(Vp/Vs)= -0.04, approximately the laboratory velocities for unfractured metagraywacke (Fig. 6) (Okaya et al., 1995; Christensen, 1996). Because dVp and d(Vp/Vs) are with respect to a 1-D profile that varies with depth, we are implicitly assuming that the velocity of unfractured rock varies with depth as well. The choice of a depth-independent unfractured rock velocity would not change the lateral variability in fracture-induced porosity but would change the absolute porosity. We estimate a lateral change of \sim 3% in the volume of fractures across the Marlborough region at 8 km depth, with volume fraction increasing towards the south in the Kaikōura area, coincident with a region of elevated earthquake density (Fig. 8; see Fig. S4 & S5 for other depths). A similar amplitude variation in fracture porosity occurring over a few kilometers is observed using ultrasonic techniques on schist, mylonite and other laboratory samples from the Alpine Fault and adjacent regions (Simpson et al., 2020).

Diverse processes such as increased fluid over-pressure or multiple different aspect ratio fractures can change the inferred fracture density. Fluid over-pressure elevates Vp/Vs, therefore leading to an overestimate of fracture concentration. Whereas most of the Marlborough upper-crustal faults do overlie a deeper region of overpressured fluid (Eberhart-Phillips and Bannister, 2010), the broad region of overpressurization is unable to explain the lateral differences in observed upper crustal Vp and Vp/Vs near the Marlborough faults. Alternatively, recorded observations of dVp and d(Vp/Vs) can be attributed to multiple different aspect ratio in-

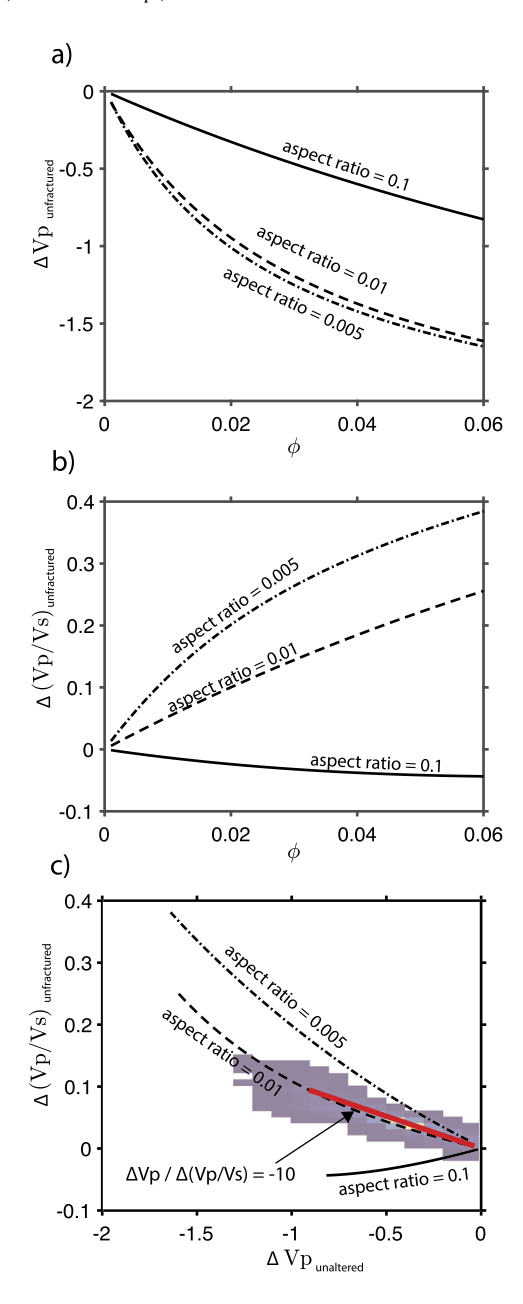


Fig. 7. Plots showing a) $\Delta Vp_{unfractured}$ and b) $\Delta (Vp/Vs)_{unfractured}$ as a function of fluid-filled fracture fraction (ϕ) , as well as c) $\Delta Vp_{unfractured}$ vs $\Delta (Vp/Vs)_{unfractured}$ for these fluid-filled fracture fractions (Kim et al., 2019a). Different line styles show results for different aspect ratio fractures. $\Delta Vp_{unfractured}$ and $\Delta (Vp/Vs)_{unfractured}$ are relative to the velocities of unfractured rocks, not the 1-D averages. Red line shows a 10:1 amplitude perturbation in Vp relative to Vp/Vs, matching that of the observations shown as a heat-map plot, after Fig. 6.

clusions. For example, rather than appealing to 0.01 aspect ratio inclusions, one could instead appeal to a combination of 0.1 and 0.005 aspect ratio inclusions, potentially changing the inferred total fracture concentration by 50% (Fig. S6). However, even though a combination of 0.1 and 0.005 aspect ratio inclusions changes the absolute fracture concentration, it does not change the *relative* lateral variation in fracture concentration, as perturbations in seismic velocities are linearly related to fracture concentration at the small volumes found here.

Because the numerical model of fracturing yields a stiffness tensor that contains information on the directional dependence of seismic velocities, numerical models can also be used to make predictions for seismic anisotropy resulting from fluid-filled fractures. Assuming consistent orientation of imposed fractures with near-vertical dip, such modeling predicts increases in azimuthal anisotropy with increases in fracture concentration. Observations from a shear-wave splitting study find an increase in azimuthal anisotropy, as measured by delay times, with increases in Vp/Vs ratio for seismic stations located within the Torlesse-Pahau terrain (Graham et al., 2020), as expected for fracture-induced anisotropy (Fig. S7). While a modest portion of this observed anisotropy may also result from folding and layering of bedding planes, laboratory-scale samples of unfractured Torlesse graywacke are nearly isotropic (Okaya et al., 1995), suggesting that a substantial portion of the observed anisotropy is due to fracturing as opposed to being intrinsic. In order to match delay times using only 0.01 aspect ratio fracture concentrations (i.e. assuming no intrinsic anisotropy), we require that fractures exist only across a thickness of <3 km (Fig. S8), with these fractures likely occurring at shallow depths as the anisotropy amplitude does not seem to depend on earthquake depth (Graham et al., 2020, and citations therein). If fractures of a given orientation extended across a larger depth range, then there would be greater delay times and higher associated anisotropy (Fig. S8). It is not clear how to reconcile the inferred fracture porosity from tomography at depths greater than 3 km (e.g. Fig. 8, shown at 8 km depth) with the lack of a corresponding delay time. One potential explanation is that fractures at depth need not share a consistent orientation, and hence may not produce an anisotropic signal, and therefore would not be observed in the shear wave delay times. Another potential explanation is that the delay times are most sensitive to the last segment of their ray path (e.g., Rümpker and Silver, 1998).

The above observations and modeling suggest that this region is characterized by extensive, fluid-filled fracturing, with decreasing fracture content away from the Kaikōura area (Fig. 9). This pattern was likely developed and fractures accumulated over multiple seismic cycles and not solely as a result of the 2016 Kaikoura sequence. While the 2016 sequence did show a temporal velocity change with decreased velocities near the rupture area, the decreases were 2 orders of magnitude too small to explain our observations (Kortink, 2020; Madley et al., 2022). Over geologic timescales, the crust is evolving as evidenced by the rupture of several previously unrecognized, immature, developing faults during the Kaikōura earthquake (Litchfield et al., 2018). Additionally, seismic catalogs show that the southern portion of Marlborough has exhibited extensive, distributed seismicity that has not historically been observed in the northern portion of the Torlesse-Pahau terrain (Fig. 8), highlighting how pervasive fractures may accumulate in certain regions over geologic time.

4.3. Sources of variability in fracture concentration

Regional variability in fracture concentration is often driven by the presence and availability of fluids as well as differences in where and how strain is accommodated. Fluid loss from the underlying Pacific plate may explain the presence and availability of crustal fluids under the Marlborough faults, which in turn may facilitate the development of major strike slip faults (Eberhart-Phillips and Reyners, 1997; Wannamaker et al., 2009). However, the mechanism does not explain why faults are younger to the south, nor the broad pattern of inferred upper-crustal fracture distribution. We therefore consider where and how strain is accommodated, while also acknowledging that regional differences in sources and volumes of fluid may play a role in fault rupture and regional fracture evolution.

Collectively, the Marlborough fault system is associated with a broad region of shear that locally accommodates most of the relative plate motion between the Pacific and Australian Plates (Bibby, 1976; Bourne et al., 1998a, 1998b; Ellis et al., 2017; Haines and Wallace, 2020). Geodetic studies also show that the shear

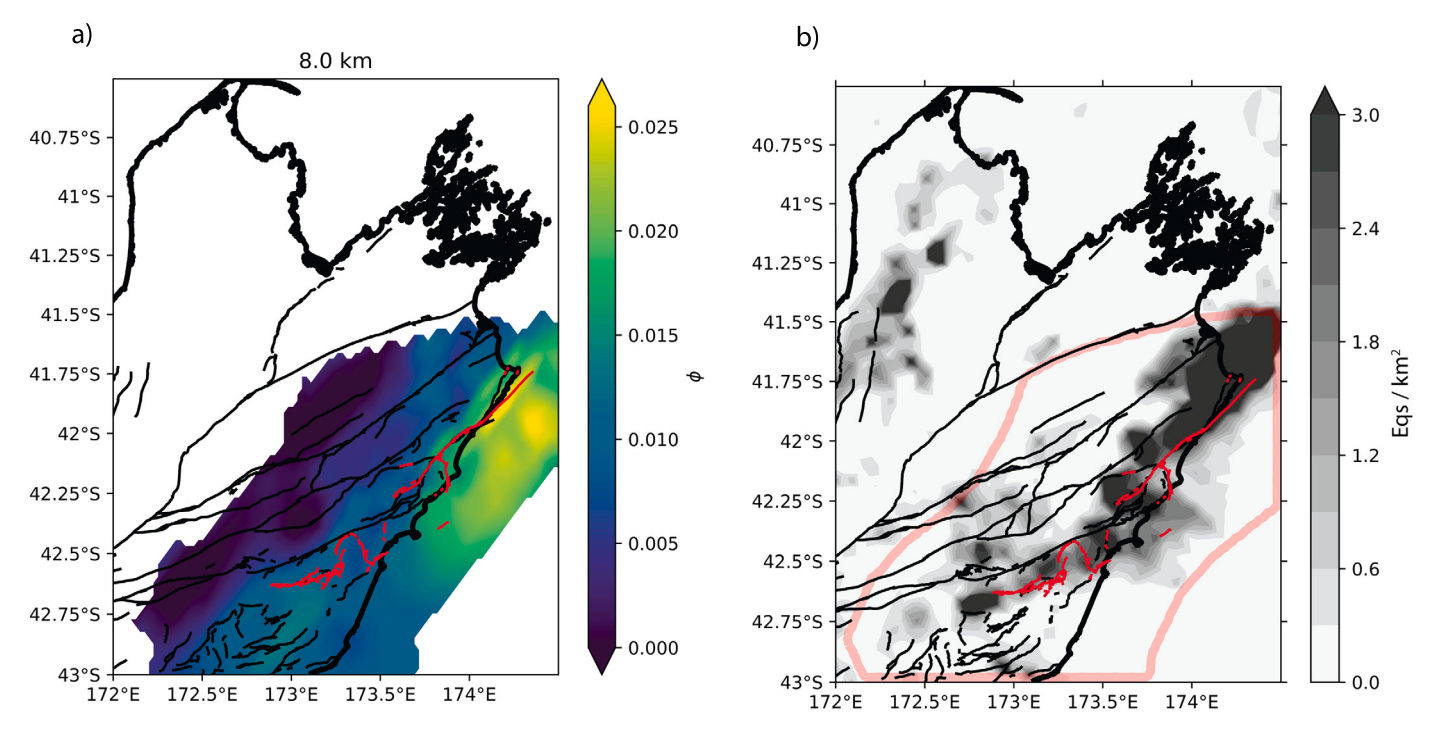


Fig. 8. (a) Modeled fluid-filled fracture fraction at 8 km depth. Elevated fluid-filled fracture amounts are observed in close proximity to faults activated during the Kaikōura earthquake. (b) Earthquake density plot, with all recorded earthquakes since 1900 less than 20 km depth. Outlined region in red marks the Torlesse-Pahau terrain. Elevated earthquake density occurs in areas near the Kaikōura rupture, highlighting broad, distributed deformation. See Fig. S5 for earthquake density plot excluding aftershocks of the Kaikōura earthquake.

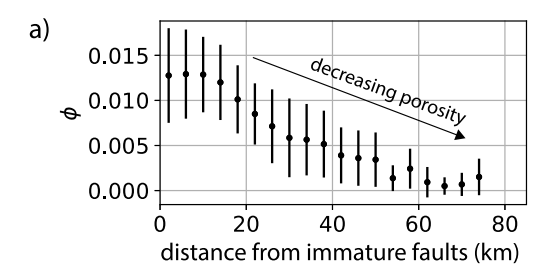
strain rate is approximately constant, decreasing only south of the Kaikōura rupture (Bourne et al., 1998a, 1998b; Lamb et al., 2018; Haines and Wallace, 2020) (Figs. 9 and S9). This broad region of near uniform shear is interpreted to be driven by locking of the megathrust, which in turn may facilitate complex crustal faulting (Lamb et al., 2018). Regionally elevated fracture concentrations are not due to increased compression or extension as the areal strain rate pattern (sum of diagonal elements of strain rate tensor, which measures the change in area) (Haines and Wallace, 2020) does not match the inferred spatial distribution of crustal fracturing (Fig. S9). We conclude that the regional variability in fracture concentration in the Marlborough region is not driven by differences in where strain is accommodated and are therefore left to investigate how the strain is accommodated.

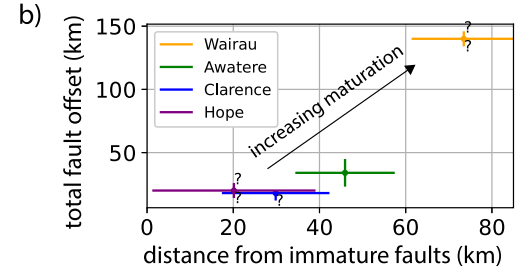
How strain is accommodated is likely influenced by a number of different parameters including: (a) composition, (b) degree of strain partitioning, and (c) fault zone maturity (Tikoff and Teyssier, 1994; Faulkner et al., 2010; Dolan and Haravitch, 2014). Based on arguments presented above, we do not consider composition to be a viable explanation for the variability in style of strain accommodation due to the relatively uniform regional lithology.

The degree of strain partitioning may affect the distribution of fractures. The local (\sim 5 km scale) surface manifestation of the observed right-lateral transpressive strain is split between various faults such that surface strike-slip motion occurs on the main faults whereas thrust faulting is located on laterally offset faults (Nicol and Van Dissen, 2002), leading to a broader distribution of fractures in areas with higher strain partitioning. Geodetic studies have inferred a partitioning from strike-slip to thrust faulting near the seaward extent of the Hope Fault (Bibby, 1981). However more recent work suggests that substantial contraction, associated with partitioned thrust faulting, is limited predominantly to the offshore region northeast of the South Island (Haines and Wallace, 2020) (Fig. S9) and therefore cannot entirely explain our results in the region.

We examine the influence of fault maturity, including fault age and total accumulated fault slip, on the distribution of fractures (see Text S2 for discussion of slip rate). On a geologic timescale, deformation has only recently transferred to the Kaikoura area, within the past few million years (Yeats and Berryman, 1987; Walcott, 1998; Little and Jones, 1998). In general, with increased proximity to the Kaikōura area, fault zones young and have smaller accumulated displacement, decreasing in age from north to south across Marlborough (Fig. 9). Areas of increased fracturing in our analysis correlate with increased proximity to the less mature fault zones (see Fig. 9). These differences in maturation of fault zones are inferred to impact the extent of fracturing. Well-developed, more mature fault zones can more efficiently accommodate strain along individual faults, in contrast to less mature fault zones that accommodate strain across multiple, distributed faults (Cowie et al., 1995). At regional scales, aftershocks from large, complicated earthquakes in immature settings highlight complex networks of faults at different scales, that distribute deformation across a broad region, often extending kilometers away from the main rupture (Bannister et al., 2006; Eberhart-Phillips and Bannister, 2010; Syracuse et al., 2013; Ross et al., 2017; Lanza et al., 2019; Shelly, 2020; Eberhart-Phillips et al., 2021). These aftershocks outline faults that are, in many cases, oriented obliquely, and sometimes even orthogonally, to the main rupture orientation (Ross et al., 2017; Shelly, 2020). Complex earthquakes therefore may be better thought of as the amalgamation of immature individual faults rupturing together in a throughgoing earthquake as opposed to a single rupture of a major fault.

At smaller scales, fault immaturity is commonly associated with a relative increase in off-fault deformation near individual faults both within the Marlborough region as well as globally (Dolan and Haravitch, 2014; Zinke et al., 2015). This correlation persists even after accounting for the association of fault immaturity with complex fault geometries, which also increases off-fault damage (Dolan and Haravitch, 2014). We therefore hypothesize that the difference in the style of strain accommodation between imma-





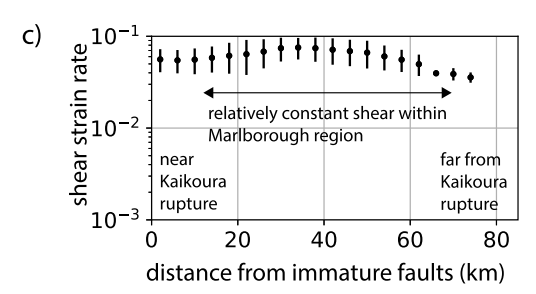


Fig. 9. (a) Modeled fluid-filled fracture concentration (ϕ) as a function of distance from immature faults (purple line in Fig. 5d) for well resolved nodes (blue dots in Fig. 5d). More immature areas (i.e., in the Kaikōura area) are characterized by elevated concentrations of fluid-filled fractures compared to regions further away. (b) Total offset of major faults in the Marlborough region (Little and Jones, 1998 and citations therein) as a function of distance to immature faults (purple line in Fig. 5d) shown with error bars. Less mature areas are characterized by smaller total fault offsets than more mature areas. Question marks denote quantities with unknown errors. (c) Shear strain rate (Haines and Wallace, 2020) as a function of distance to immature areas.

ture and mature fault zones is causing the difference in fracture concentration, with immature fault zones associated with broadly distributed, pervasive fractures, at scales ranging from regionally distributed faulting/fracturing (> tens of km) to individual off-fault deformation zones surrounding individual faults (>1 m) (Fig. 10). This elevated fracturing may in turn facilitate the migration of fluids into the upper crust.

A complication to this hypothesis is seen in the relatively modest fracture-induced porosities for the very immature faults south of the Kaikōura rupture, which should be among the regions of highest fracturing. It is not clear precisely why fracture-induced porosity is only modest here, but one plausible explanation is that the regional maturation is influenced by the tectonic shear strain rate, which is anomalously low in this area compared to the near-uniform shear rate of the rest of the Marlborough region (Fig. S9). Such a change could impact fracture distribution, volume, aspect ratio as well as fault strain rate. Also, this region is not as well resolved (Fig. S3). A thorough analysis of this region is outside the scope of this paper.

4.4. Relationship between fault zone maturity, fracture distribution, and fluid distribution

Models of fault formation, growth, and maturation inform the lateral variation in fracture concentration observed in this study. In numerical models and laboratory experiments, faults form through

the interaction and coalescence of microfractures, wherein rocks initially stressed exhibit a broad distribution of fractures that eventually localize to form a through-going fault, with through-going faults ultimately coalescing to form fault zones (Reches and Lockner, 1994; Cowie et al., 1995). Prior to fault initiation, fracturing is distributed broadly, yielding no clear evidence where the main fault will eventually form (Reches and Lockner, 1994). Maturation of faults continues with increased net fault displacement, leading to progressive localization of slip along individual fault cores and smoothing of faults, reducing the number of step-overs per unit length (Wesnousky, 1988, 2005).

The time evolution of this fault-growth process is inferred to be represented in the lateral distribution of fractures within the Marlborough terrain. In this model, fewer overall open fractures are present in the regions near the mature fault zones, as the system has efficiently localized deformation along the high-strain fault core. In contrast, younger, less mature faults with less displacement are rougher and are inefficiently localizing strain along the fault core, instead allowing for its distribution across a broad area (Kim et al., 2004; Peacock et al., 2017). This yields both a broader fracture distribution and increased off-fault deformation due to increased complexity of the fault geometry (Fig. 10) (Kim et al., 2004; Faulkner et al., 2010).

The overall complexity of the Kaikōura earthquake rupture reflects the relative immaturity of the faults in this area. Similarly, other complex earthquake ruptures occurring around the globe are associated with immature, evolving faults, such as the 1992 Landers earthquake, the 1999 Hector Mine earthquake, the 2019 Ridgecrest earthquake, and the 2020 Elazığ earthquake (Milliner et al., 2016; Goldberg et al., 2020; Gallovič et al., 2020). On a more regional scale, comparison between the immature Walker Lane fault system and the more mature San Andreas system shows the immature Walker Lane to be more complex, with a broader fault distribution (Wesnousky, 2005).

One assumption of this model is that, as faults mature, the fractures formed during the immature phase of fault evolution tend to close, fill, or heal over some amount of geologic time. Without such a process, fractures from the immature stage of fault development would continue to exist throughout maturation (Fig. 10). Fault healing, which is commonly observed after earthquakes, often results in reduced fracture concentration from processes such as crack closure, compaction, and healing of microcracks (Morrow and Byerlee, 1989; Brantley et al., 1990; Sleep and Blanpied, 1992; Segall and Rice, 1995; Li and Vidale, 2001; Li et al., 2004). It is not clear which of these processes operate in the Marlborough region.

5. Conclusion

We used P arrival times and S-P arrival time differences from earthquakes as well as active source data around the Marlborough region of New Zealand's South Island to image 3D Vp and Vp/Vs variations, focusing on the Torlesse-Pahau terrane that encompasses the region in which multiple faults ruptured during the 2016 Kaikōura earthquake. We found anomalously low Vp and anomalously high Vp/Vs in the Marlborough terrain for regions near the Kaikōura rupture, with higher Vp and lower Vp/Vs further away from the rupture (to the north). Uniformity of lithology within this terrane suggests that the lateral variations in Vp and Vp/Vs are not due to compositional variations and instead are due to differences in fracture concentration. Using numerical models of the effect of fractures on Vp and Vp/Vs and comparing to the imaged Vp and Vp/Vs variations, we infer an increased fracture concentration in the Kaikoura portion of the Marlborough region relative to areas further north. We estimate lateral differences of up to 3% fracture induced porosity difference caused by \sim 0.01 aspect ratio fractures, favoring the interpretation that re-

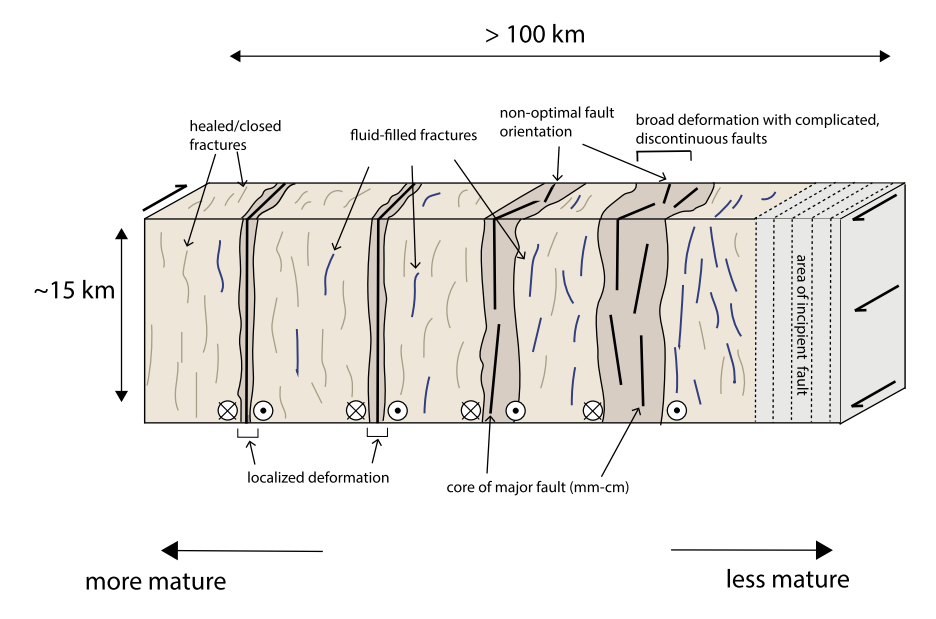


Fig. 10. Conceptual representation of the maturation process observed in Marlborough along right-lateral faults that mature from right to left in the figure. Major faults are characterized by an efficient localization of deformation along a fault core. Within the crust near major faults, there are associated fractures. In more mature regions, such fractures have healed and deformation is more efficiently localized along the fault core, yielding lower regional concentrations of fluid-filled fractures in the surrounding region. Regions associated with less mature major faults are characterized by extensive fluid-filled fractures away from the fault core that have not healed, and have broader regions of deformation with non-optimally oriented, complicated fault surfaces.

gionally increased fracturing is related to fault immaturity within the uniformly sheared Marlborough terrain. We infer that the more mature faults in the north portion of Marlborough efficiently accommodate strain, leading to a lower regional fracture concentration. In contrast, the less mature faults to the south near the Kaikōura rupture are early in the process of developing and are associated with higher amounts of off-fault deformation, more irregular and complex fault geometries, and broader, more pervasive regional fractures.

CRediT authorship contribution statement

Ben Heath – Conceptualization, Investigation, Writing. **Donna Eberhart-Phillips** – Conceptualization, Investigation, Writing.

Federica Lanza - Conceptualization, Investigation, Editing.

Clifford Thurber – Conceptualization, Investigation, Writing, Supervision.

Martha Savage - Conceptualization, Investigation, Editing.

Tomomi Okada – Investigation: data collection.

Satoshi Matsumoto - Investigation: data collection.

Yoshihisa Iio - Investigation: data collection.

Stephen Bannister - Investigation.

Declaration of competing interest

The authors confirm that there are no known conflicts of interest associated with this publication and there has been no significant financial support for this work that could have influenced its outcome.

Acknowledgements

Constructive comments and reviews by Jack Williams, Rebecca Bendick, and an anonymous reviewer greatly improved the quality of the manuscript. This work was supported by NSF award EAR-1756075, by funding from the New Zealand Earthquake Commission (EQC grant number: 18/755), and by a Grant-in-Aid for Special Purposes (15H05206), MEXT, Japan. This work was also

partly supported by the Scientific Research Program on Innovative Areas, "Crustal Dynamics" at Kyoto University (2608), and by the Ministry of Education, Culture, Sports, Science and Technology (MEXT) of Japan, under its Observation and Research Program for Prediction of Earthquakes and Volcanic Eruptions. Waveform and earthquake catalog data from GeoNet are available from http://www.geonet.org.nz. BH would also like to acknowledge the late Eunyoung Kim for her friendship and scientific curiosity.

Appendix A. Supplementary material

Supplementary material related to this article can be found online at https://doi.org/10.1016/j.epsl.2022.117666.

References

Bannister, S., Thurber, C., Louie, J., 2006. Detailed fault structure highlighted by finely relocated aftershocks, Arthur's Pass, New Zealand. Geophys. Res. Lett. 33. https://doi.org/10.1029/2006GL027462.

Bibby, H.M., 1976. Crustal strain across the Marlborough faults, New Zealand. N.Z. J. Geol. Geophys. 19, 407–425. https://doi.org/10.1080/00288306.1976.10423537.

Bibby, H.M., 1981. Geodetically determined strain across the southern end of the Tonga-Kermadec-Hikurangi subduction zone. Geophys. J. R. Astron. Soc. 66, 513–533. https://doi.org/10.1111/j.1365-246X.1981.tb04888.x.

Bourne, S.J., Árnadóttir, T., Beavan, J., Darby, D.J., England, P.C., Parsons, B., Walcott, R.I., Wood, P.R., 1998a. Crustal deformation of the Marlborough Fault Zone in the South Island of New Zealand: geodetic constraints over the interval 1982-1994. J. Geophys. Res., Solid Earth 103, 30147–30165. https://doi.org/10.1029/98]B02228.

Bourne, S.J., England, P.C., Parsons, B., 1998b. The motion of crustal blocks driven by flow of the lower lithosphere and implications for slip rates of continental strike-slip faults. Nature 391, 655–659. https://doi.org/10.1038/35556.

Brantley, S.L., Evans, B., Hickman, S.H., Crerar, D.A., 1990. Healing of microcracks in quartz: implications for fluid flow. Geology 18, 136. https://doi.org/10.1130/0091-7613(1990)018<0136:HOMIQI>2.3.CO;2.

Christensen, N.I., 1996. Poisson's ratio and crustal seismology. J. Geophys. Res., Solid Earth 101, 3139–3156. https://doi.org/10.1029/95JB03446.

Cowie, P.A., Sornette, D., Vanneste, C., 1995. Multifractal scaling properties of a growing fault population. Geophys. J. Int. 122, 457–469. https://doi.org/10.1111/ j.1365-246X.1995.tb07007.x.

Crampin, S., 1986. Anisotropy and transverse isotropy. Geophys. Prospect. 34, 94–99. https://doi.org/10.1111/j.1365-2478.1986.tb00454.x.

Dolan, J.F., Haravitch, B.D., 2014. How well do surface slip measurements track slip at depth in large strike-slip earthquakes? The importance of fault structural

- maturity in controlling on-fault slip versus off-fault surface deformation. Earth Planet. Sci. Lett. 388, 38–47. https://doi.org/10.1016/j.epsl.2013.11.043.
- Eberhart-Phillips, D., Bannister, S., 2010. 3-D imaging of Marlborough, New Zealand, subducted plate and strike-slip fault systems. Geophys. J. Int. 182, 73–96. https://doi.org/10.1111/j.1365-246X.2010.04621.x.
- Eberhart-Phillips, D., Bannister, S., 2015. 3-D imaging of the northern Hikurangi subduction zone, New Zealand: variations in subducted sediment, slab fluids and slow slip. Geophys. J. Int. 201, 838–855. https://doi.org/10.1093/gji/ggv057.
- Eberhart-Phillips, D., Ellis, S., Lanza, F., Bannister, S., 2021. Heterogeneous material properties—as inferred from seismic attenuation—influenced multiple fault rupture and ductile creep of the Kaikoura Mw 7.8 earthquake, New Zealand. Geophys. J. Int. 227, 1204–1227. https://doi.org/10.1093/gji/ggab272.
- Eberhart-Phillips, D., Henderson, M.C., 2004. Including anisotropy in 3-D velocity inversion and application to Marlborough, New Zealand. Geophys. J. Int. 156, 237–254. https://doi.org/10.1111/j.1365-246X.2003.02044.x.
- Eberhart-Phillips, D., Reyners, M., 1997. Continental subduction and three-dimensional crustal structure: the northern South island, New Zealand. J. Geophys. Res., Solid Earth 102, 11843–11861. https://doi.org/10.1029/96JB03555.
- Eberhart-Phillips, D., Reyners, M., 2012. Imaging the Hikurangi Plate interface region, with improved local-earthquake tomography. Geophys. J. Int. 190, 1221–1242. https://doi.org/10.1111/j.1365-246X.2012.05553.x.
- Eberhart-Phillips, D., Han, D.-H., Zoback, M.D., 1989. Empirical relationships among seismic velocity, effective pressure, porosity, and clay content in sandstone. Geophysics 54, 82–89. https://doi.org/10.1190/1.1442580.
- Ellis, S., Van Dissen, R., Eberhart-Phillips, D., Reyners, M., Dolan, J.F., Nicol, A., 2017.

 Detecting hazardous New Zealand faults at depth using seismic velocity gradients. Earth Planet. Sci. Lett. 463, 333–343. https://doi.org/10.1016/j.epsl.2017.01.

 038.
- Faulkner, D.R., Jackson, C.A.L., Lunn, R.J., Schlische, R.W., Shipton, Z.K., Wibberley, C.A.J., Withjack, M.O., 2010. A review of recent developments concerning the structure, mechanics and fluid flow properties of fault zones. J. Struct. Geol. 32, 1557–1575. https://doi.org/10.1016/j.jsg.2010.06.009.
- Gallovič, F., Zahradník, J., Plicka, V., Sokos, E., Evangelidis, C., Fountoulakis, I., Turhan, F., 2020. Complex rupture dynamics on an immature fault during the 2020 Mw 6.8 Elazığ earthquake, Turkey. Commun. Earth Environ. 1, 40. https://doi.org/10.1038/s43247-020-00038-x.
- Goldberg, D.E., Melgar, D., Sahakian, V.J., Thomas, A.M., Xu, X., Crowell, B.W., Geng, J., 2020. Complex rupture of an immature fault zone: a simultaneous kinematic model of the 2019 Ridgecrest, CA earthquakes. Geophys. Res. Lett. 47, e2019GL086382. https://doi.org/10.1029/2019GL086382.
- Graham, K.M., Savage, M.K., Arnold, R., Zal, H.J., Okada, T., Iio, Y., Matsumoto, S., 2020. Spatio-temporal analysis of seismic anisotropy associated with the Cook Strait and Kaikõura earthquake sequences in New Zealand. Geophys. J. Int. 223, 1987–2008. https://doi.org/10.1093/gji/ggaa433.
- Haines, A.J., Wallace, L.M., 2020. New Zealand-wide geodetic strain rates using a physics-based approach. Geophys. Res. Lett. 47. https://doi.org/10.1029/2019GL084606.
- Hamling, I.J., et al., 2017. Complex multifault rupture during the 2016 Mw 7.8 Kaikōura earthquake, New Zealand. Science 356. https://doi.org/10.1126/science.aam7194
- Henrys, S., et al., 2020. Upper plate heterogeneity along the Southern Hikurangi margin, New Zealand. Geophys. Res. Lett. 47. https://doi.org/10.1029/2019G1085511
- Hudson, J.A., 2000. The effect of fluid pressure on wave speeds in a cracked solid. Geophys. J. Int. 143, 302–310. https://doi.org/10.1046/j.1365-246X.2000.01239.x.
- Kerrich, R., 1986. Fluid infiltration into fault zones: chemical, isotopic, and mechanical effects. Pure Appl. Geophys. 124, 225–268. https://doi.org/10.1007/ RF00875727
- Kim, E., Kim, Y., Mainprice, D., 2019a. GassDem: a MATLAB program for modeling the anisotropic seismic properties of porous medium using differential effective medium theory and Gassmann's poroelastic relationship. Comput. Geosci. 126, 131–141. https://doi.org/10.1016/j.cageo.2019.02.008.
- Kim, Y.S., Peacock, D.C.P., Sanderson, D.J., 2004. Fault damage zones. J. Struct. Geol. 26, 503–517. https://doi.org/10.1016/j.jsg.2003.08.002.
- Kim, E., Toomey, D.R., Hooft, E.E.E., Wilcock, W.S.D., Weekly, R.T., Lee, S.M., Kim, Y.H., 2019b. Upper crustal Vp/Vs ratios at the Endeavour segment, Juan de Fuca Ridge, from joint inversion of P and S traveltimes: implications for hydrothermal circulation. Geochem. Geophys. Geosyst. 20, 208–229. https://doi.org/10.1029/2018GC007921.
- Knuepfer, P.L.K., 1992. Temporal variations in latest Quaternary slip across the Australian-Pacific plate boundary, northeastern South Island, New Zealand. Tectonics 11, 449–464.
- Kortink, M.A., 2020. Effects of the Kaikoura earthquake on velocity changes in and around the ruptured region: a noise cross-correlation approach. Masters Thesis. Victoria University of Wellington. 151 p.
- Lamb, S., Arnold, R., Moore, J.D.P., 2018. Locking on a megathrust as a cause of distributed faulting and fault-jumping earthquakes. Nat. Geosci. 11, 871–875. https://doi.org/10.1038/s41561-018-0230-5.
- Lanza, F., et al., 2019. Crustal fault connectivity of the Mw 7.8 2016 Kaikōura earth-quake constrained by aftershock relocations. Geophys. Res. Lett. 46, 6487–6496. https://doi.org/10.1029/2019GL082780.

- Li, Y.-G., Vidale, J.E., 2001. Healing of the shallow fault zone from 1994-1998 after the 1992 M 7.5 Landers, California, earthquake. Geophys. Res. Lett. 28, 2999–3002. https://doi.org/10.1029/2001GL012922.
- Li, Y.-G., Vidale, J.E., Cochran, E.S., 2004. Low-velocity damaged structure of the San Andreas Fault at Parkfield from fault zone trapped waves. Geophys. Res. Lett. 31. https://doi.org/10.1029/2003GL019044.
- Litchfield, N.J., et al., 2018. Surface rupture of multiple crustal faults in the 2016 Mw 7.8 Kaikōura, New Zealand, earthquake. Bull. Seismol. Soc. Am. 108, 1496–1520. https://doi.org/10.1785/0120170300.
- Little, T.A., Jones, A., 1998. Seven million years of strike-slip and related off-fault deformation, northeastern Marlborough fault system, South Island, New Zealand. Tectonics 17, 285–302. https://doi.org/10.1029/97TC03148.
- Madley, M., Yates, A., Savage, M., Wang, W., Okada, T., Matsumoto, S., lio, Y., Jacobs, K., 2022. Velocity changes around the Kaikoura earthquake ruptures from ambient noise cross-correlations. Geophys. J. Int. 229, 1357–1371.
- Mainprice, D., 1997. Modelling the anisotropic seismic properties of partially molten rocks found at mid-ocean ridges. Tectonophysics 279, 161–179. https://doi.org/ 10.1016/S0040-1951(97)00122-4.
- McCaig, A.M., 1988. Deep fluid circulation in fault zones. Geology 16, 867. https://doi.org/10.1130/0091-7613(1988)016<0867:DFCIFZ>2.3.CO;2.
- Milliner, C.W.D., Dolan, J.F., Hollingsworth, J., Leprince, S., Ayoub, F., 2016. Comparison of coseismic near-field and off-fault surface deformation patterns of the 1992 M_w 7.3 Landers and 1999 M_w 7.1 Hector Mine earthquakes: Implications for controls on the distribution of surface strain. Geophys. Res. Lett. 43, 10115–10124. https://doi.org/10.1002/2016G1069841.
- Morrow, C.A., Byerlee, J.D., 1989. Experimental studies of compaction and dilatancy during frictional sliding on faults containing gouge. J. Struct. Geol. 11, 815–825.
- Nicol, A., Van Dissen, R., 2002. Up-dip partitioning of displacement components on the oblique-slip Clarence Fault, New Zealand. J. Struct. Geol. 24, 1521–1535. https://doi.org/10.1016/S0191-8141(01)00141-9.
- Okada, T., et al., 2019. Comparative tomography of reverse-slip and strike-slip seismotectonic provinces in the northern South Island, New Zealand. Tectonophysics 765, 172–186. https://doi.org/10.1016/j.tecto.2019.03.016.
- Okaya, D., Christensen, N., Stanley, D., Stern, T., South Island Geophysical Transect, 1995. Crustal anisotropy in the vicinity of the Alpine Fault Zone, South Island, New Zealand. N.Z. J. Geol. Geophys. 38, 579–583. https://doi.org/10.1080/00288306.1995.9514686
- Paulatto, M., Moorkamp, M., Hautmann, S., Hooft, E., Morgan, J.V., Sparks, R.S.J., 2019. Vertically extensive magma reservoir revealed from joint inversion and quantitative interpretation of seismic and gravity data. J. Geophys. Res., Solid Earth 124, 11170–11191. https://doi.org/10.1029/2019JB018476.
- Peacock, D.C.P., Dimmen, V., Rotevatn, A., Sanderson, D.J., 2017. A broader classification of damage zones. J. Struct. Geol. 102, 179–192. https://doi.org/10.1016/j.jsg. 2017.08.004.
- Peacock, S., Hudson, J.A., 1990. Seismic properties of rocks with distributions of small cracks. Geophys. J. Int. 102, 471–484. https://doi.org/10.1111/j.1365-246X.
- Rattenbury, M.S., Townsend, D.B., Johnston, M.R., 2006. Geology of the Kaikoura Area. Institute of Geological & Nuclear Sciences. v. 13, 1–71.
- Reches, Z., Lockner, D.A., 1994. Nucleation and growth of faults in brittle rocks. J. Geophys. Res., Solid Earth 99, 18159–18173. https://doi.org/10.1029/94JB00115.
- Rice, J.R., 1992. Fault stress states, pore pressure distributions, and the weakness of the San Andreas fault. In: International Geophysics. Elsevier, pp. 475–503.
- Ross, Z.E., Hauksson, E., Ben-Zion, Y., 2017. Abundant off-fault seismicity and orthogonal structures in the San Jacinto fault zone. Sci. Adv. 3, e1601946. https://doi.org/10.1126/sciadv.1601946.
- Rümpker, G., Silver, P.G., 1998. Apparent shear-wave splitting parameters in the presence of vertically varying anisotropy. Geophys. J. Int. 135, 790–800. https://doi.org/10.1046/j.1365-246X.1998.00660.x.
- Segall, P., Rice, J.R., 1995. Dilatancy, compaction, and slip instability of a fluid-infiltrated fault. J. Geophys. Res., Solid Earth 100, 22155–22171. https://doi.org/10.1029/95IB02403.
- Shelly, D.R., 2020. A high-resolution seismic catalog for the initial 2019 Ridgecrest earthquake sequence: Foreshocks, aftershocks, and faulting complexity. Seismol. Res. Lett. 91, 1971–1978. https://doi.org/10.1785/0220190309.
- Shillington, D.J., Van Avendonk, H.J.A., Behn, M.D., Kelemen, P.B., Jagoutz, O., 2013. Constraints on the composition of the Aleutian arc lower crust from Vp/Vs. Geophys. Res. Lett. 40, 2579–2584. https://doi.org/10.1002/grl.50375.
- Sibson, R.H., 2020. Dual-driven fault failure in the lower seismogenic zone. Bull. Seismol. Soc. Am. 110, 850–862. https://doi.org/10.1785/0120190190.
- Simpson, J., Adam, L., Wijk, K., Charoensawan, J., 2020. Constraining microfractures in foliated Alpine fault rocks with laser ultrasonics. Geophys. Res. Lett. 47. https://doi.org/10.1029/2020GL087378.
- Sleep, N.H., Blanpied, M.L., 1992. Creep, compaction and the weak rheology of major faults. Nature 359, 687–692.
- Syracuse, E.M., Thurber, C.H., Rawles, C.J., Savage, M.K., Bannister, S., 2013. High-resolution relocation of aftershocks of the Mw 7.1 Darfield, New Zealand, earth-quake and implications for fault activity. J. Geophys. Res., Solid Earth 118, 4184–4195. https://doi.org/10.1002/jgrb.50301.
- Takei, Y., 2002. Effect of pore geometry on Vp/Vs: From equilibrium geometry to crack. J. Geophys. Res. 107, 2043. https://doi.org/10.1029/2001JB000522.

- Thurber, C., Eberhart-Phillips, D., 1999. Local earthquake tomography with flexible gridding. Comput. Geosci. 25, 809–818. https://doi.org/10.1016/S0098-3004(99)
- Thurber, C., Roecker, S., Ellsworth, W., Chen, Y., Lutter, W., Sessions, R., 1997. Two-dimensional seismic image of the San Andreas fault in the Northern Gabilan Range, central California: evidence for fluids in the fault zone. Geophys. Res. Lett. 24, 1591–1594. https://doi.org/10.1029/97GL01435.
- Tikoff, B., Teyssier, C., 1994. Strain modeling of displacement-field partitioning in transpressional orogens. J. Struct. Geol. 16, 1575–1588. https://doi.org/10.1016/0191-8141(94)90034-5
- Ulrich, T., Gabriel, A.-A., Ampuero, J.-P., Xu, W., 2019. Dynamic viability of the 2016 Mw 7.8 Kaikōura earthquake cascade on weak crustal faults. Nat. Commun. 10, 1213. https://doi.org/10.1038/s41467-019-09125-w.
- Walcott, R.I., 1998. Modes of oblique compression: Late Cenozoic tectonics of the South Island of New Zealand. Rev. Geophys. 36, 1–26. https://doi.org/10.1029/ 97RC03084
- Wannamaker, P.E., Caldwell, T.G., Jiracek, G.R., Maris, V., Hill, G.J., Ogawa, Y., Bibby, H.M., Bennie, S.L., Heise, W., 2009. Fluid and deformation regime of an advancing subduction system at Marlborough, New Zealand. Nature 460, 733–736. https://doi.org/10.1038/nature08204.
- Wesnousky, S.G., 1988. Seismological and structural evolution of strike-slip faults. Nature 335, 340–343.

- Wesnousky, S.G., 2005. The San Andreas and Walker lane fault systems, western North America: transpression, transtension, cumulative slip and the structural evolution of a major transform plate boundary. J. Struct. Geol. 27, 1505–1512. https://doi.org/10.1016/j.jsg.2005.01.015.
- Williams, J.N., Toy, V.G., Massiot, C., McNamara, D.D., Wang, T., 2016. Damaged beyond repair? Characterising the damage zone of a fault late in its interseismic cycle, the Alpine fault, New Zealand. J. Struct. Geol. 90, 76–94. https:// doi.org/10.1016/j.jsg.2016.07.006.
- Yeats, R.S., Berryman, K.R., 1987. South Island, New Zealand, and Transverse Ranges, California: a seismotectonic comparison. Tectonics 6, 363–376.
- Zandt, G., Ammon, C.J., 1995. Continental crust composition constrained by measurements of crustal Poisson's ratio. Nature 374, 152–154. https://doi.org/10.1038/374152a0.
- Zhang, H., Thurber, C., Bedrosian, P., 2009. Joint inversion for Vp, Vs, and Vp/Vs at SAFOD, Parkfield, California. Geochem. Geophys. Geosyst. 10. https://doi.org/10.1029/2009GC002709.
- Zinke, R., Dolan, J.F., Van Dissen, R., Grenader, J.R., Rhodes, E.J., McGuire, C.P., Langridge, R.M., Nicol, A., Hatem, A.E., 2015. Evolution and progressive geomorphic manifestation of surface faulting: a comparison of the Wairau and Awatere faults, South Island, New Zealand. Geology 43, 1019–1022. https://doi.org/10.1130/G37065.1.